Supporting information for

Fe-Porphyrin-derived Carbon Nanofiber-based Nanozymes: Enhanced Peroxidase-like Activity for Ultrasensitive Glucose and Ascorbic Acid Sensing

*Pradeep Singh Thakur,[a] and Muniappan Sankar,[a,b]**

[1]Centre for Nanotechnology, Indian Institute of Technology Roorkee, Roorkee-247667, India

[2]Department of Chemistry, Indian Institute of Technology Roorkee, Roorkee-247667, India

***Corresponding author:** E-mail: *m.sankar@cy.iitr.ac.in*; Tel: +91-1332-284753

Table of Contents	**Page No.**

INSTRUMENTATIONS AND METHODS

The Absorption spectra were recorded using SHIMADZU UV–vis spectrophotometer (UV-2600) using a pair of quartz cells of 3.5 mL volume and 10 mm path length. MALDI- TOF mass spectra were recorded on a Bruker UltrafleXtreme-TN MALDI-TOF/TOF mass spectrometer. ^{1}H NMR spectra were recorded on a JEOL 500 MHz NMR spectrometer with ECZ500R/S1 model. The chemical shifts (d) are expressed in ppm with Me_4Si as an internal standard (d = 0 ppm) in the respective deuterated solvents. The field emission scanning electron microscopy (FE-SEM) images and energy dispersive X-ray spectra (EDAX) were collected from a FE-SEM, Apreo S LoVac instrument coupled with an energy-dispersive X-ray detector (EDX)

operating at an accelerating voltage of about 15–20 keV. TEM grids were prepared by placing 10 µL of the nanocomposite solution on a carbon-coated copper grid and drying at room temperature. The transmission electron microscopy (TEM) images and selected area electron diffraction (SAED) patterns were obtained from a TECNAI G2 20 S-TWIN (FEI Netherlands) microscope, operating at 200 keV. All the FESEM and TEM images were processed using ImageJ (NIH, http://rsb.info.nih.gov/ij) software. X-ray photoelectron spectroscopy (XPS) measurements were performed with the material's powder on an ESCALAB-MKII spectrometer (excitation source of 1486.6 eV).

SYNTHETIC PROCEDURES

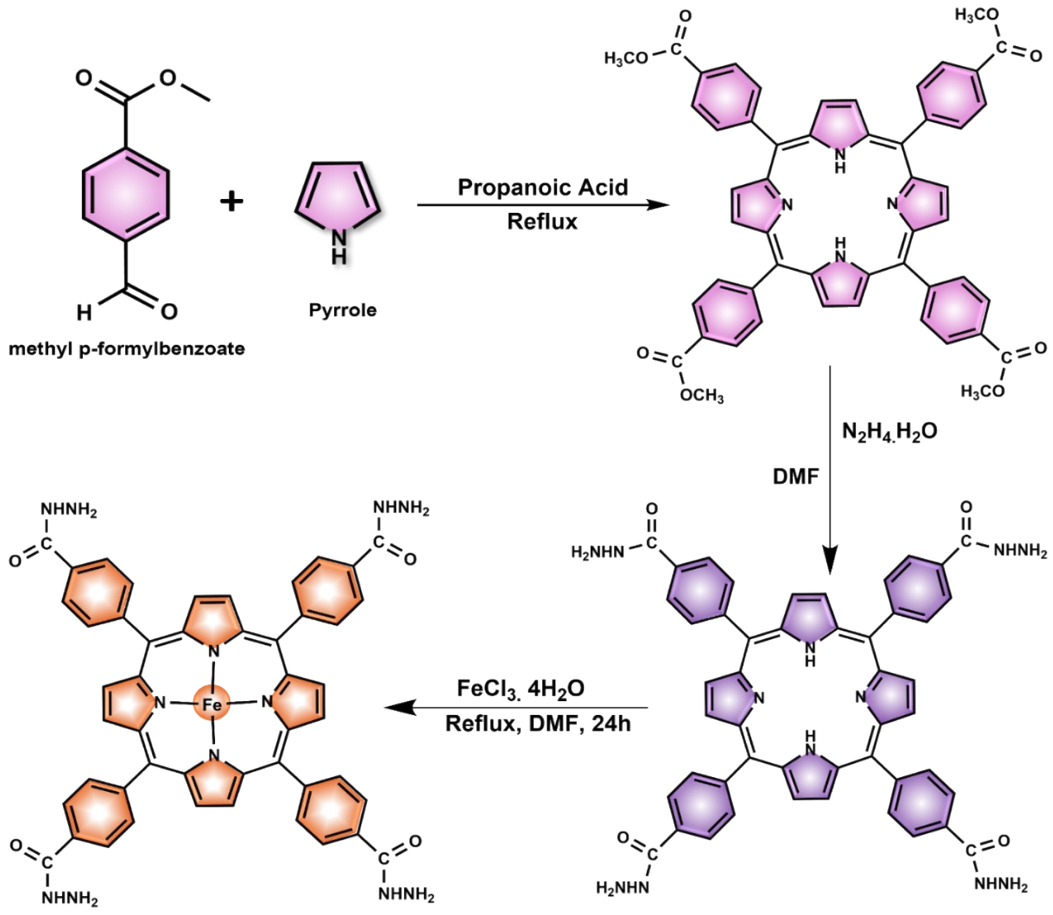

Scheme 1 Synthetic scheme for FeTHCPP.

Synthesis of *meso*–tetrakis(4–methoxycarbonylphenyl) porphyrin (TPPCOOMe)

Pyrrole (3.0 mL, 0.043 mol) and methyl p-formylbenzoate (6.9 g, 0.042 mol) were added to refluxed propionic acid (250 mL) in a 500-mL three necked flask, and the solution was refluxed for 12 hrs. After the reaction mixture was cooled to room temperature, the solution was left overnight to allow the precipitation of the porphyrins. The reaction solid was collected by filtration and washed by distilled water to remove the propionic acid. After re-crystal three times by chloroform ($CHCl_3$)/ethanol (volume ratio= 1:1) to yield purple crystals.

TPPCOOMe: Yield= 22%. UV-Vis: $CHCl_3$. (λ_{max} in nm): 419, 516, 551, 590, 646, ^{1}H NMR (400 MHz, $CDCl_3$) δ (ppm): 8.82 (s, 8H), 8.44 (d, 8H), 8.30 (d, 8H), 4.12 (s, 12H), -2.78 (s, 2H). MS (MALDI-TOF): calcd. 846.26 $[M]^+$, found 846.29.

Synthesis of *meso*-tetrakis(4-hydrazidocarbonylphenyl)porphyrin (THCPP)

meso-tetrakis(4–methoxycarbonylphenyl) porphyrin (TPPCOOMe) (100 mg) was taken in a tightly closed tube with 2 mL DMF as the solvent and 1 ml of 98% hydrazine hydrate. The mixture was refluxed at 120 ºC with stirring for 24 hours. After completion of the reaction, it was further cooled to room temperature. The precipitate thus obtained was filtered and washed with acetonitrile. The dark purple solid obtained was vacuum dried at 100 ºC and characterized further.

THCPP: Yield = 93%. UV-Vis: MeOH. (λ_{max} in nm): 417, 515, 550, 591, 650. ^{1}H NMR (500 MHz, DMSO-d_6) δ in ppm = 10.18 (s, 4H), 8.84 (s, 8H), 8.27 (AB, J_{AB} =10 Hz, 16H), 4.75 (s, 8H), -2.98 (s, 2H). MALDI-TOF-MS: m/z 846.25 for $[M]^+$ (calculated 846.31).

Synthesis of *meso*-tetrakis(4-hydrazidocarbonylphenyl)porphyrin iron (III) (FeTHCPP)

The intermediate free-base porphyrin (THCPP) was taken for iron metalation using ferric chloride (III) in DMF. The reaction mixture was refluxed for 1 day at 120 ºC. The product extracted after water wash was further confirmed by UV/vis and mass spectrum.

Fe-THCPP: Yield = 95%. UV-Vis: MeOH. (λ_{max} in nm): 418, 571, 611.MALDI-TOF-MS: m/z 900.13 for $[M]^+$ (calculated 900.23).

Preparation of Fe-porphyrin/ PAN electrospun nanofibers (Fe-P NFs)

At first, 400 mg of polyacrylonitrile (PAN) powder was dissolved in 5 mL of DMF, stirring at room temperature, to achieve a homogeneous and transparent solution. Then, 20 mg of Fe-THCPP was added into the above PAN solution with magnetic stirring overnight to obtain the viscous solution. The viscous solution as an electrospun precursor was filled into a 5 mL plastic syringe with a 0.6 mm diameter blunt-ended needle. The electrospun NFs containing Fe-porphyrin were prepared by using commercial electrospinning equipment. The electrospinning conditions were optimized to give non-beaded almost uniform nanofibers. Finally, the synthesis was performed under a voltage of 10-15 kV with a flow rate of 1ml/hour. The distance from the syringe to the collector was around 20 cm, and the ambient temperature and air humidity were 25–30 °C and 50–60%, respectively. Similarly, bare PAN-based NFs were prepared under the same conditions.

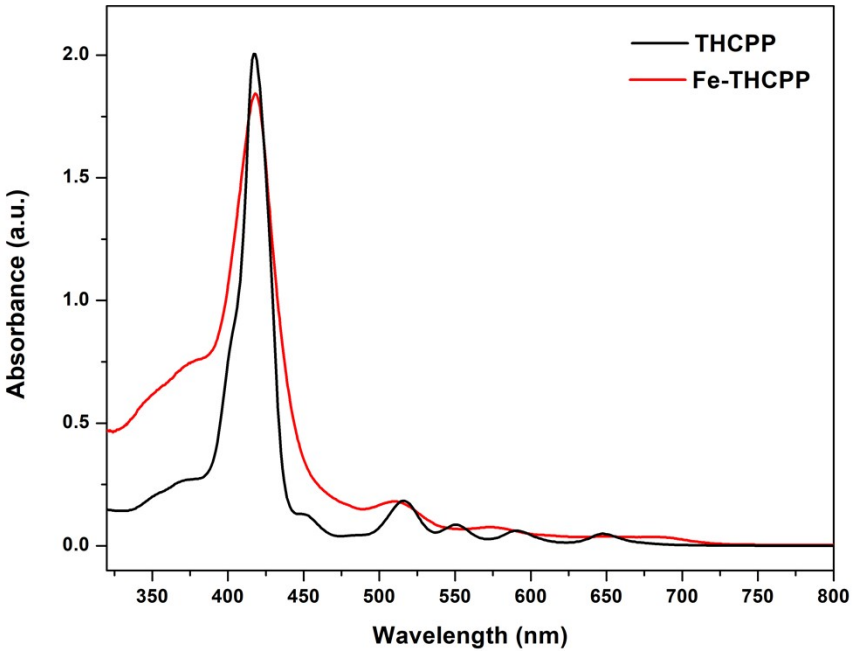

Figure S1 Comparative UV-spectrum of THCPP, and Fe-THCPP (0.1 mM in chloroform).

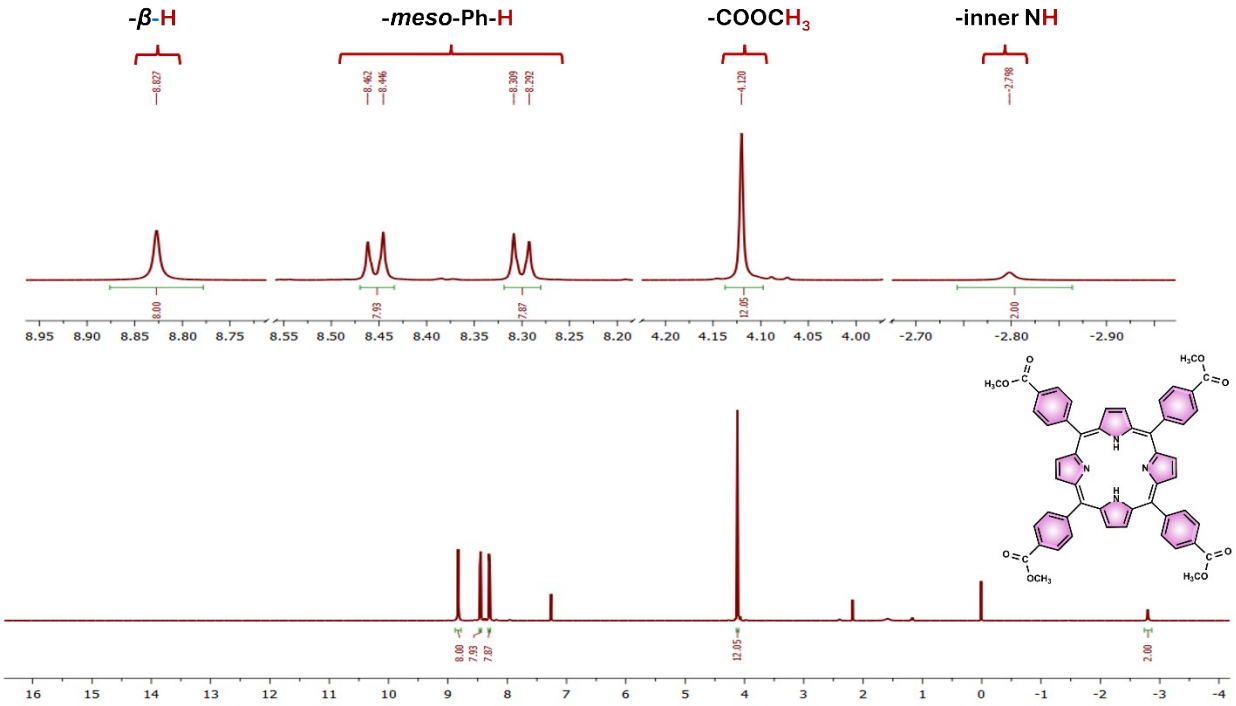

Figure S2 ^{1}H NMR spectrum of TPPCOOMe in $CDCl_3$ at 298 K.

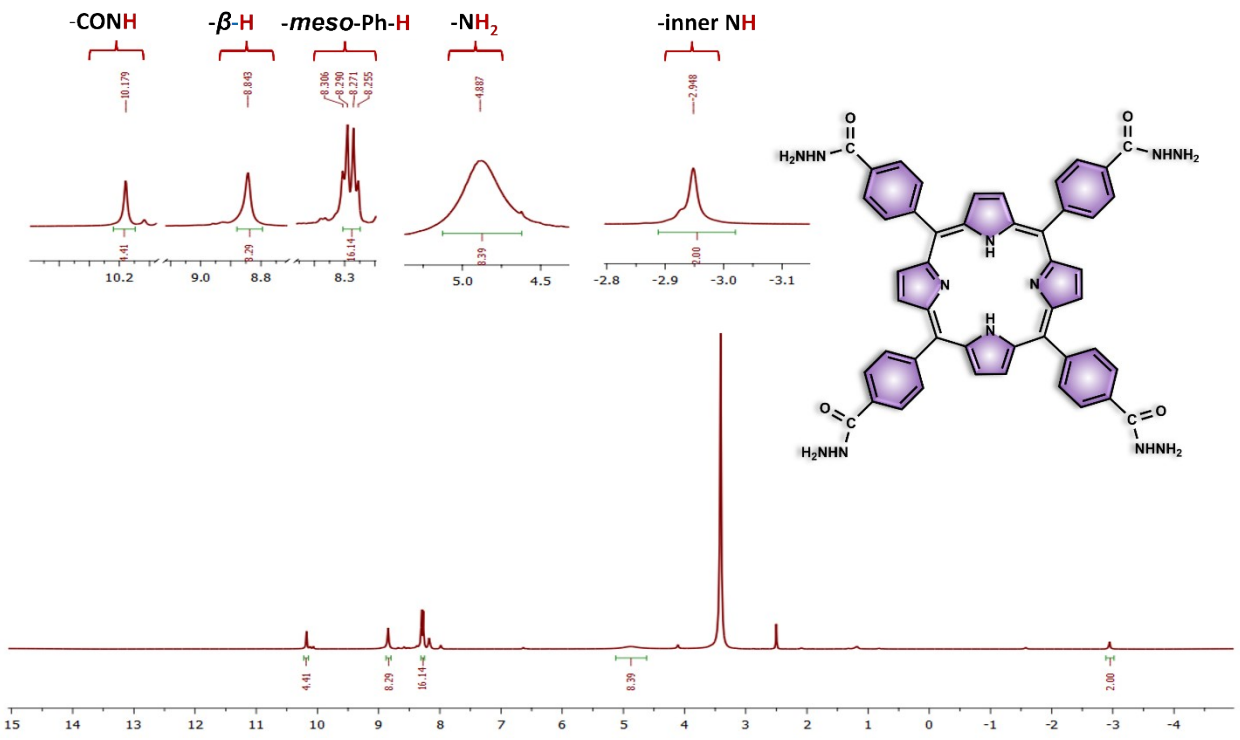

Figure S3 ^{1}H NMR spectrum of THCPP in DMSO-d_6 at 298 K.

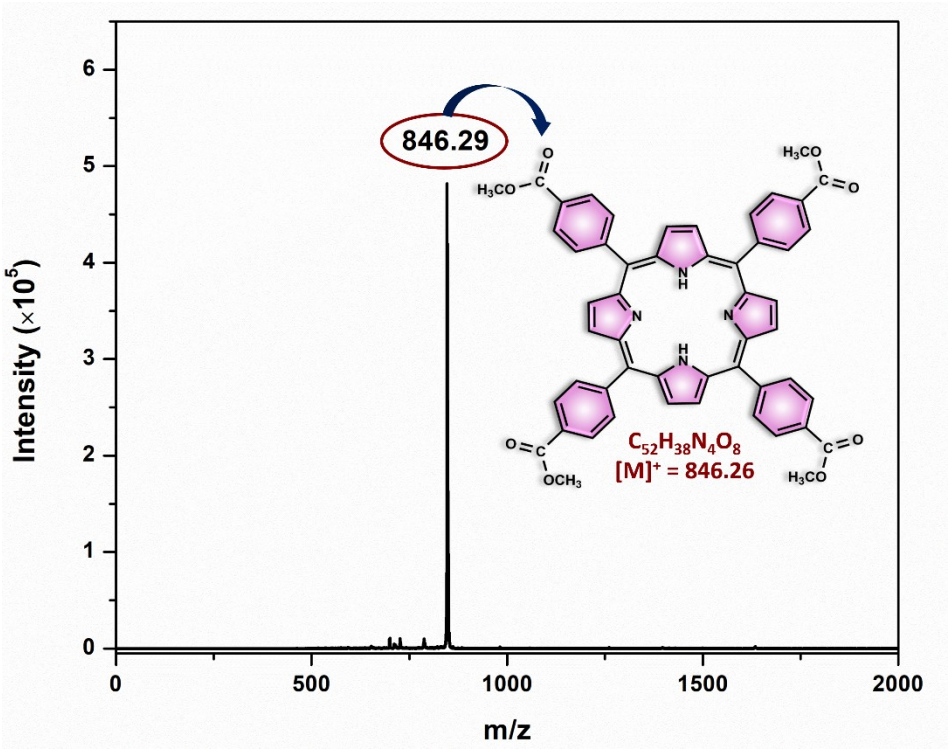

Figure S4 The MALDI-TOF-MS of TPPCOOMe in positive ion mode at 298 K.

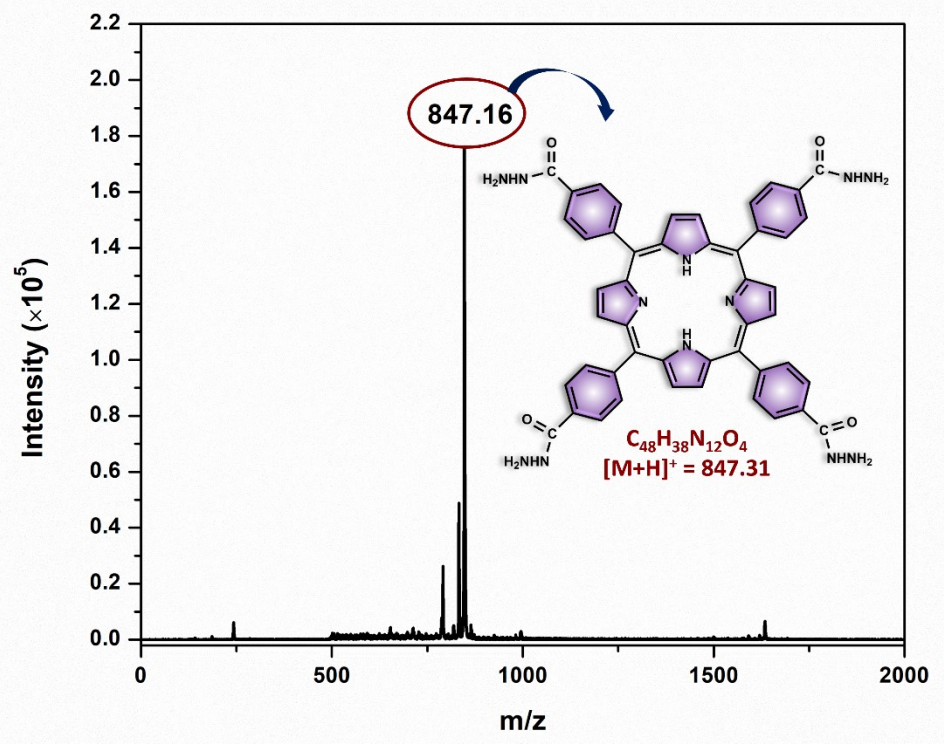

Figure S5 The MALDI-TOF-MS of THCPP in positive ion mode at 298 K.

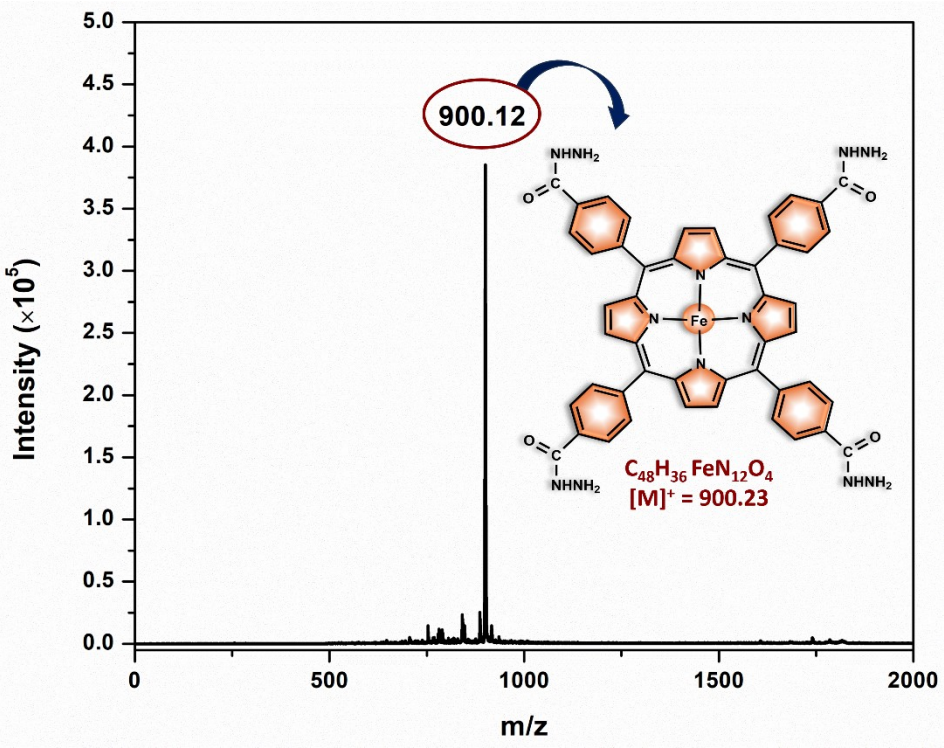

Figure S6 The MALDI-TOF-MS of Fe-THCPP in positive ion mode at 298 K.

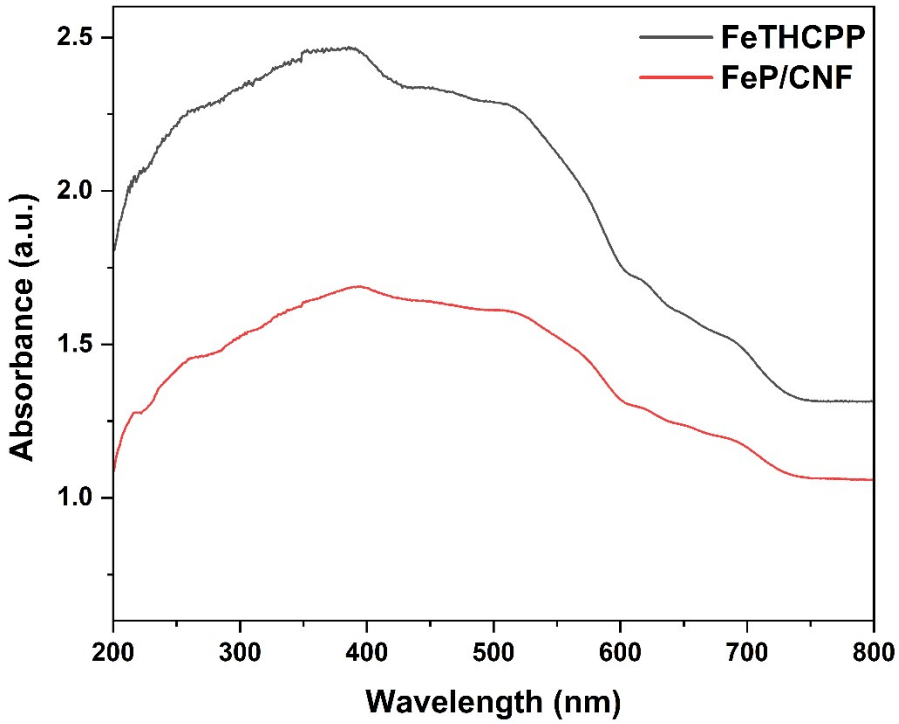

Figure S7 UV/Vis diffuse reflectance spectra (DRS) of Fe-THCPP and Fe-P/CNF.

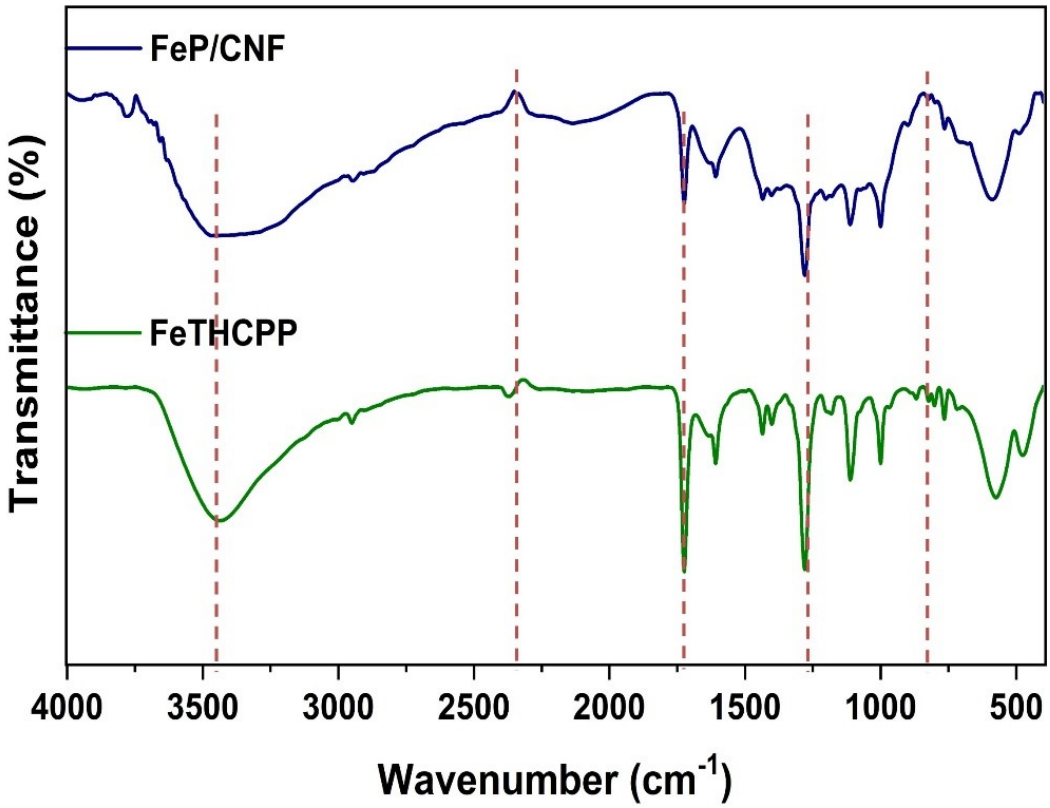

Figure S8 The FTIR spectra of Fe-THCPP and Fe-P/CNF.

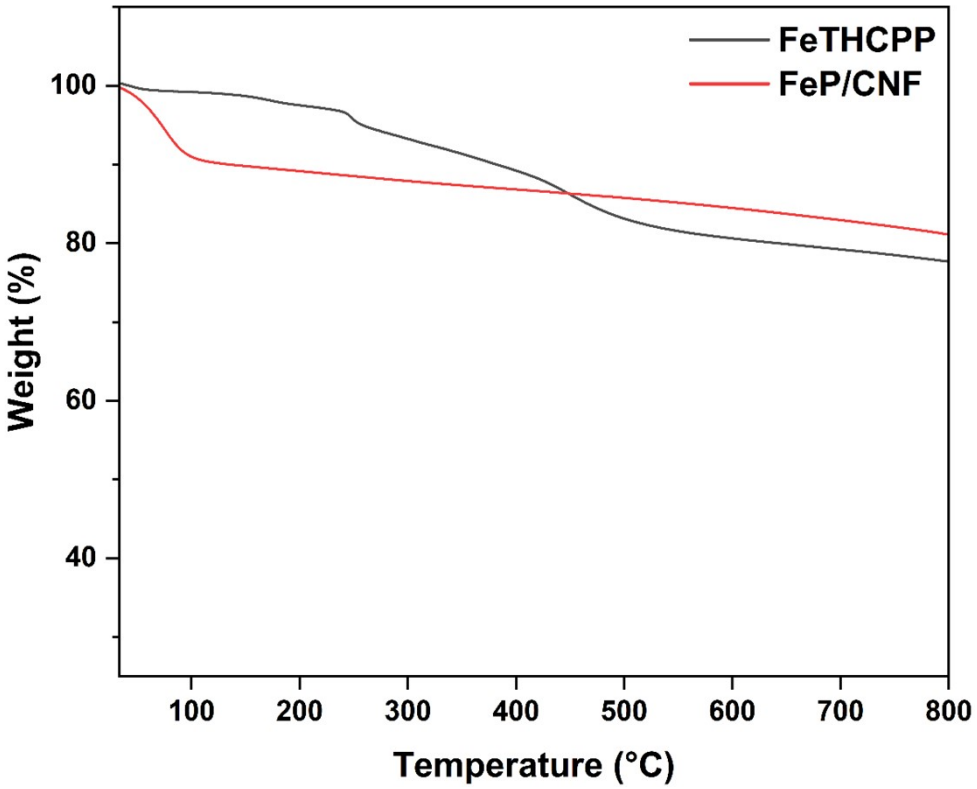

Figure S9 The TGA curves of FeTHCPP and FeP/CNF under N_2 atmosphere.

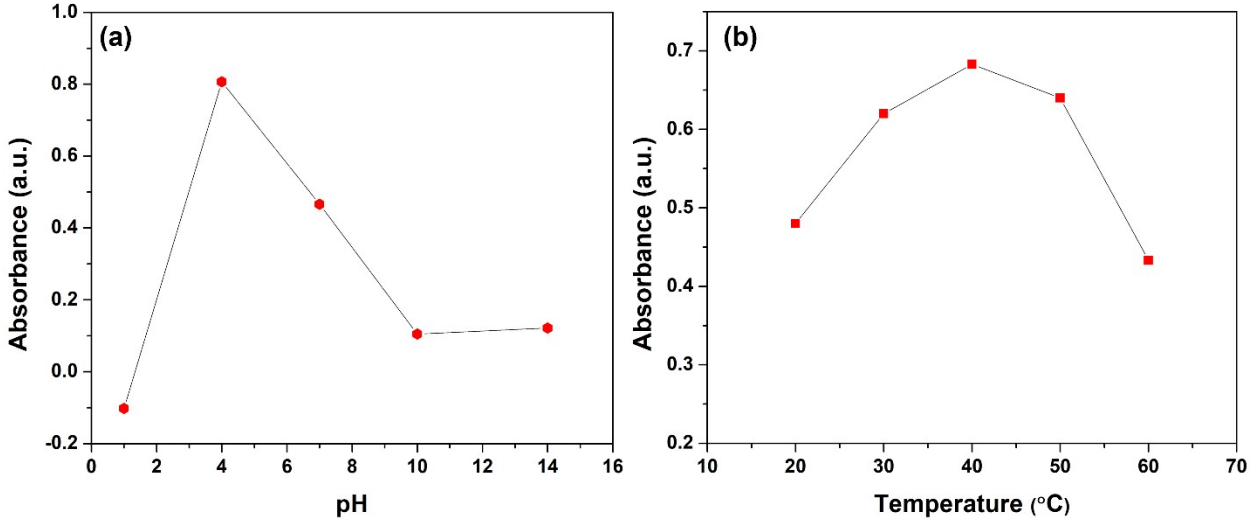

Figure S10 (a) Optimization of pH, and (b) optimization of temperature for peroxidase-like activity.

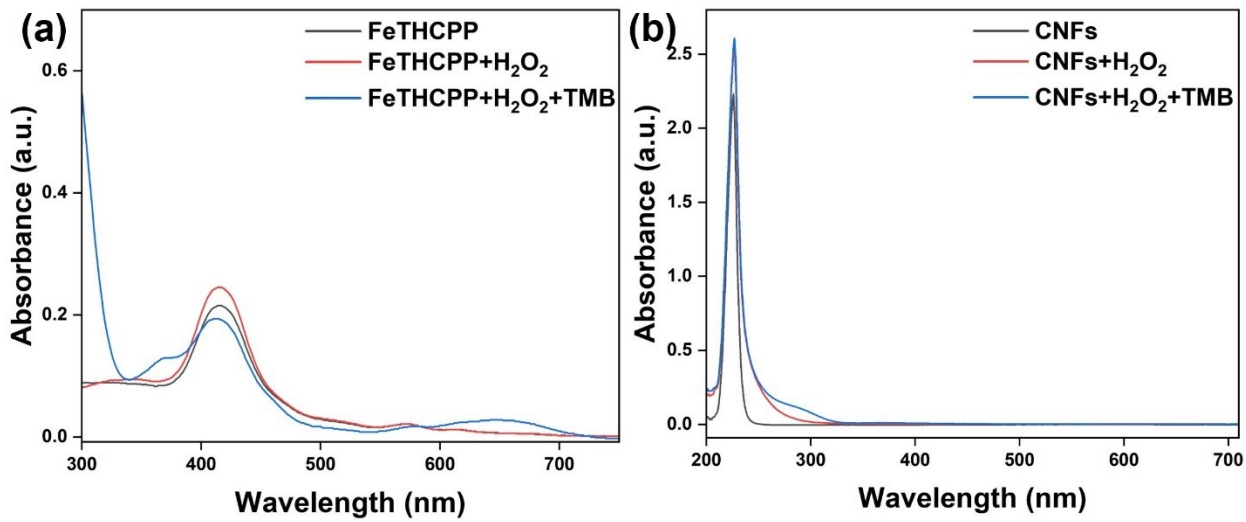

Figure S11 Analysis of peroxidase-like activity for (a) Fe-porphyrin (FeTHCPP) and (b) bare carbon nanofibers (CNFs).

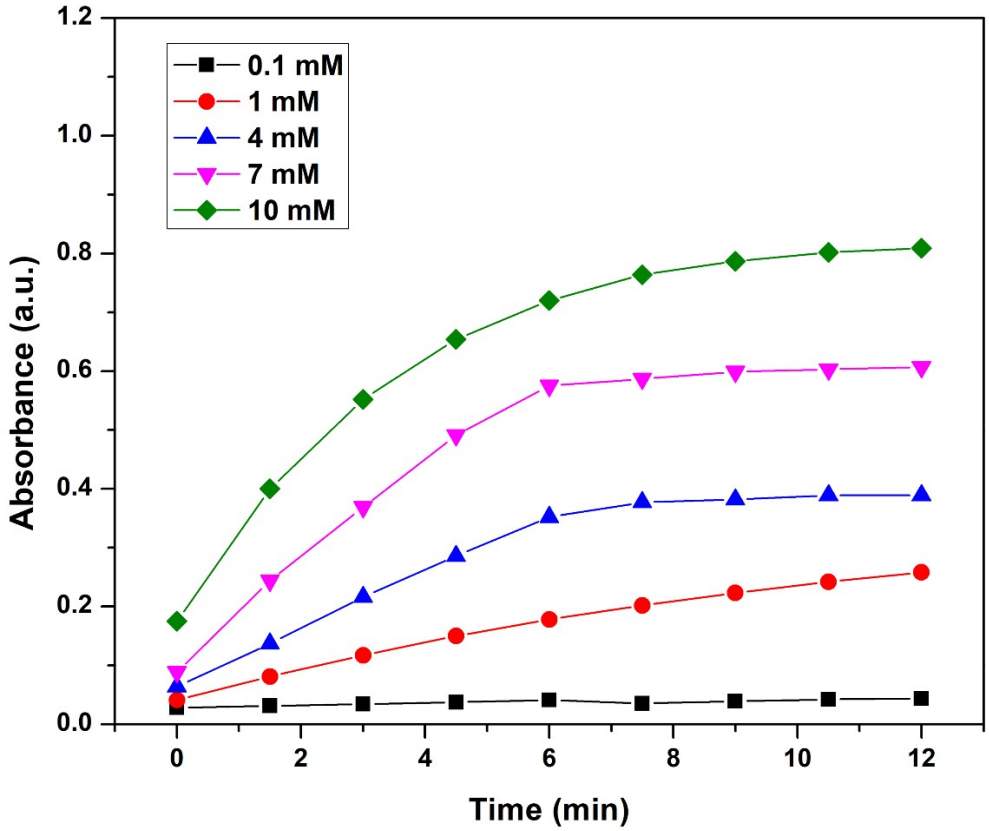

Figure S12 Plots of absorbance at 652 nm versus time during the catalytic oxidation of TMB (5 mM) by different concentrations of H_2O_2 (0.1, 1, 4, 7, and 10 mM) in presence of Fe-P/CNFs (3 mg/mL) at pH= 4.0 and 37 °C.

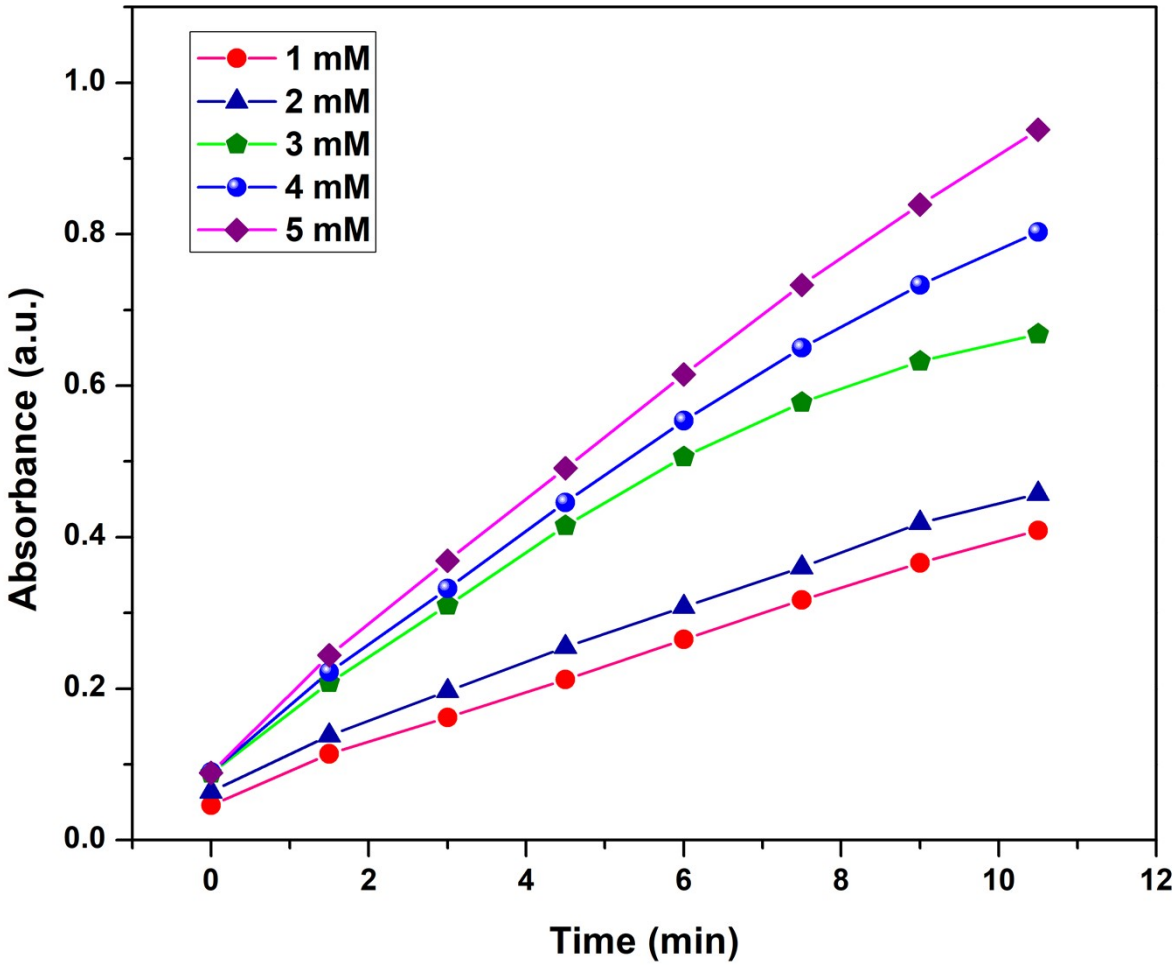

Figure S13 Plots of absorbance at 652 nm versus time during the catalytic oxidation of different concentrations of TMB (1, 2, 3, 4, and 5 mM) by H_2O_2 (10 mM) in the presence of Fe-P/CNFs (3 mg/mL) at pH= 4.0 and 37 °C.

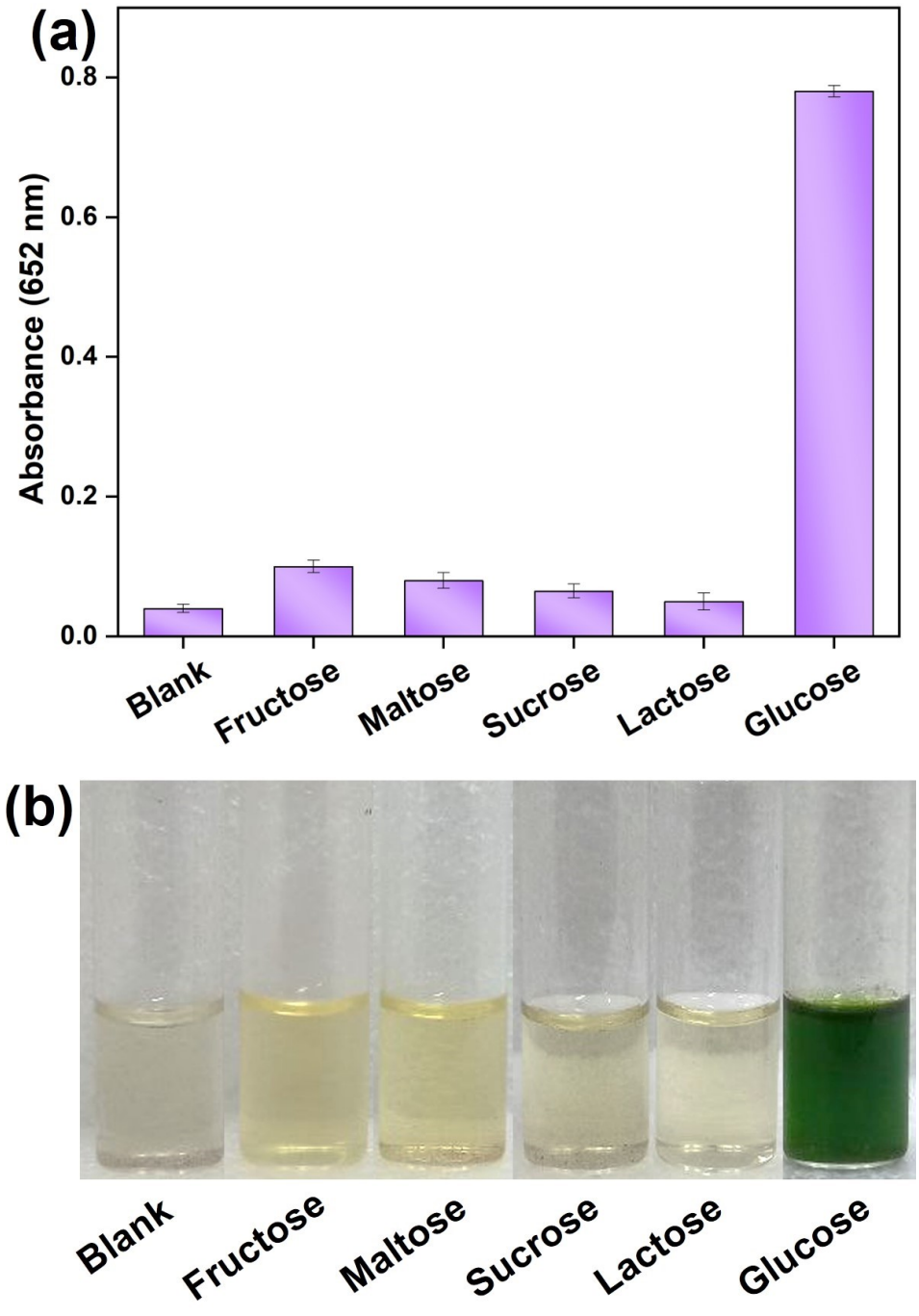

Figure S14 (a) Selectivity analysis of Fe-P/CNFs for the determination of glucose (0.2 mM), by monitoring the absorbance at 652 nm with its other analogues sucrose (2 mM), lactose (2 mM) and maltose (2 mM). (b) the corresponding color change images of different samples.

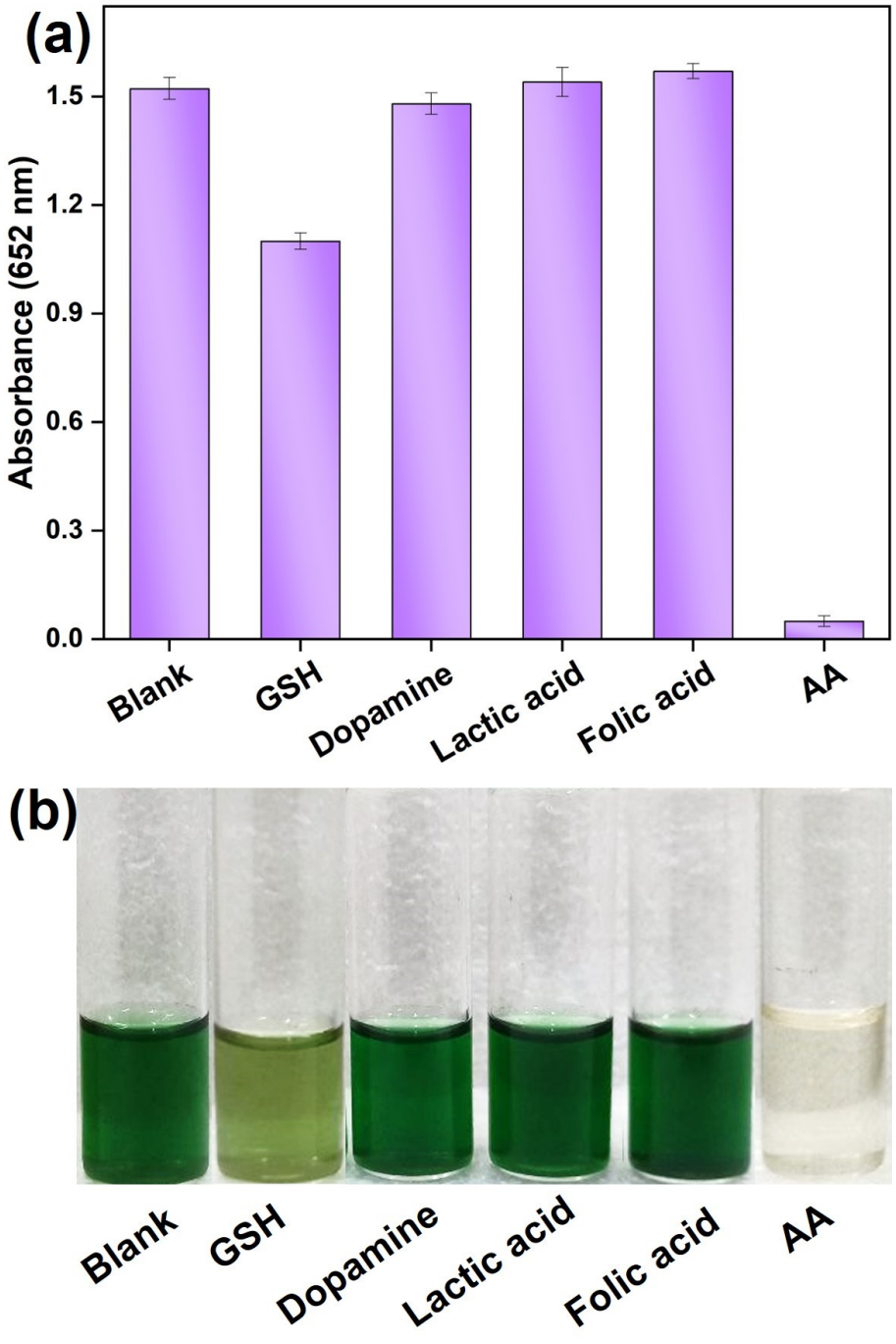

Figure S15 (a) Selectivity analysis of Fe-P/CNFs for the determination of ascorbic acid, by monitoring the absorbance at 652 nm against other potential interfering biomolecules glutathione (GSH), dopamine, lactic acid and folic acid. (b) the corresponding color change images of different samples.

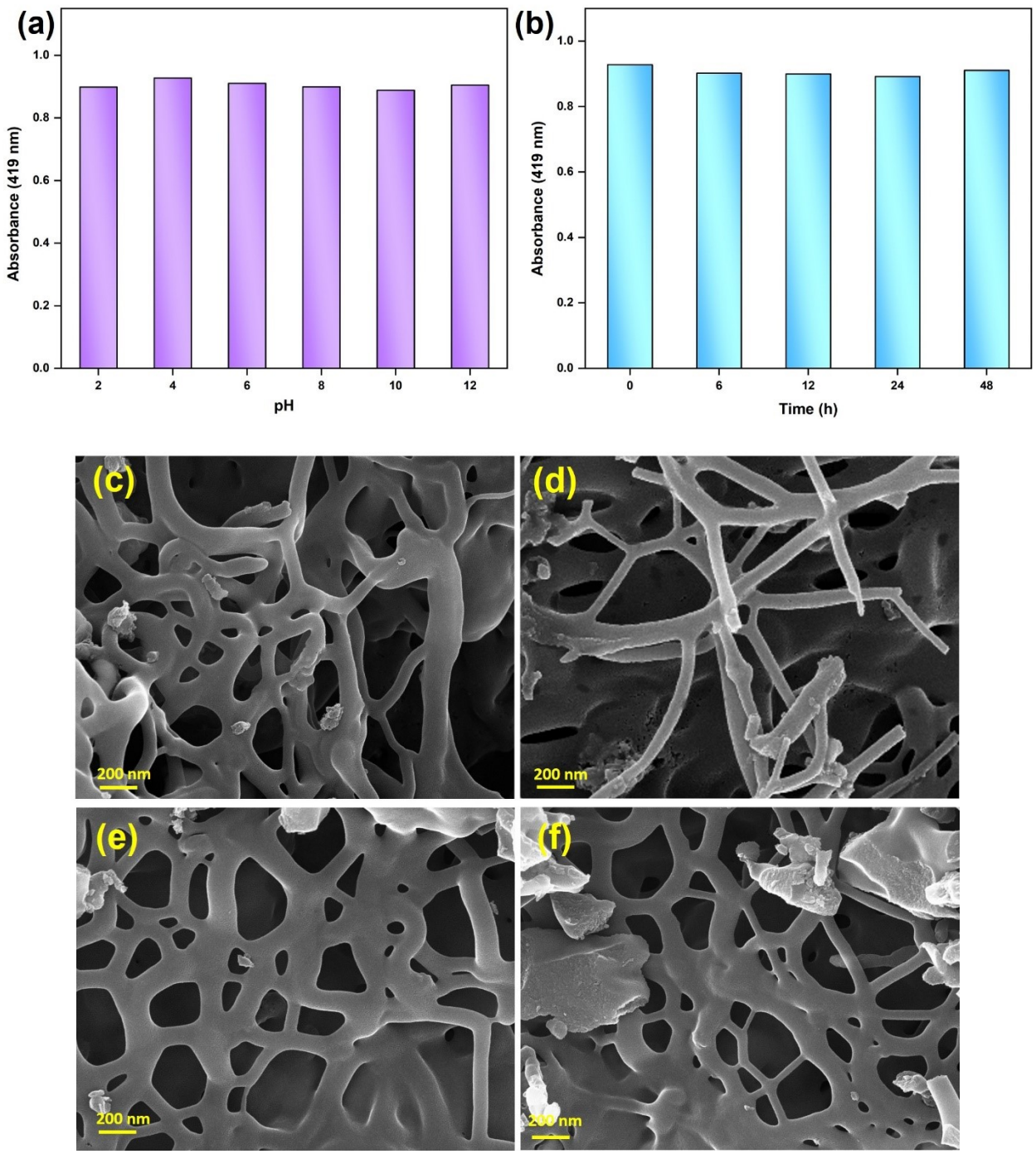

Figure S16 Stability studies of Fe-P/CNFs (a) at different pH. (b) over time at pH 4.0. FESEM images of Fe-P/CNFs at different pH (c) 2.0 (d) 4.0 (e) 7.0 and (f) 10.0.

Table S1 FTIR analysis of Fe-THCPP and Fe-P/CNF.

	Wavenumber (cm^{-1})	**Functional Group Assignment**
Fe-THCPP	3436	N–H stretching
	1724	C=O stretching
	1608	C=C stretching (aromatic) of the ring
	1279	C–N stretching
	1111	N–N stretching
	998	N–H bending vibrations
	574	Fe-N stretching in the porphyrin ring
Fe-P/CNF	3448	N–H stretching
	1724	C=O stretching
	1608	C=C stretching (aromatic) of the ring
	1277	C–O stretching
	1113	N–N stretching
	999	N–H bending vibrations
	584	Fe-N stretching in the porphyrin ring

Table S2 Comparison of kinetic parameters for TMB and H_2O_2 (K_m and V_{max}).

Catalyst	Type of Substrate	K_m (mM)	V_{max} (10^{-8} M s^{-1})	Ref.
HRP	TMB	0.434	10	[1]
	H_2O_2	3.7	8.71	
Por-$NiCo_2S_4$	TMB	0.3	34.86	[2]
	H_2O_2	4.5	4.32	
H_2TCPP-CeO_2	TMB	0.011	26.9	[3]
	H_2O_2	0.366	0.496	
H-Fe-POP	TMB	0.016	26.63	[4]
	H_2O_2	0.546	36.86	
Por/CoO/GO	TMB	0.109	10.48	[5]
	H_2O_2	5.781	5.506	
Fe-P/CNFs	TMB	2.54	5.52	This work
	H_2O_2	0.184	2.54	

Abbreviations- HRP: horseradish peroxidase; Por-$NiCo_2S_4$:porphyrin functionalized $NiCo_2S_4$ yolk-shell nanospheres: H_2TCPP: 5,10,15,20-tetrakis (4-carboxylphenyl) porphyrin; POP: porous organic polymer; GO: graphene oxide; Fe-P/CNFs: Fe-porphyrin-derived carbon nanofibers.

Table S3 Comparison of the linear range and the limit of detection for glucose detection by different nanozyme catalysts.

Porphyrin-based Nanozymes	Linear range (μM)	LOD (μM)	References
H_2TCPP-Fe_3O_4	5 – 25	2.2	[6]
H_2TCPP-ZnS NCs	5 – 500	36	[7]
H_2TCPP-CeO_2 NPs	50 –100	33	[3]
H_2TCPP-CeO_2 NRs	40 –150	19	[8]
H_2TCPP-NiO NCs	50 –500	20	[9]
Au NPs/Cu-TCPP(Fe) NSs	10 –300	8.5	[10]
Fe-Por-COF	20 –200	4.43	[11]
Fe-DMP-POR	0 –150	4.84	[12]
Fe-P/CNFs	0.02 – 200	2.55	This work

Abbreviations- H_2TCPP: 5,10,15,20-*tetrakis*(4-carboxyphenyl)-porphyrin; NPs: nanoparticles; NRs: nanorods; NCs: nanocomposites; NSs: nanosheets; Fe-Por-COF: iron porphyrin-based covalent organic framework; Fe-DMP-POR: Fe(III)-porphyrin-based covalent organic polymer Fe-P/CNFs: Fe-porphyrin-derived carbon nanofibers.

Table S4 Comparison of the catalyst with other sensing platforms for ascorbic acid detection.

Catalyst	Linear range (μM)	LOD (μM)	References
Co-POP	20 – 400	1.60	[13]
Co-CQDs	10 – 400	18	[14]
Fe-POP	4 – 24	0.11	[15]
Fe-POP	2 – 26	0.33	[16]
Fe-P/CNFs	10 – 90	0.17	This work

Abbreviations- POP: porous organic polymer; CQDs: carbon quantum dots; Fe-P/CNFs: Fe-porphyrin-derived carbon nanofibers.

References

1 L. Gao, J. Zhuang, L. Nie, J. Zhang, Y. Zhang, N. Gu, T. Wang, J. Feng, D. Yang, S. Perrett and X. Yan, *Nat. Nanotechnol.*, 2007, **2**, 577–583.

2 Y. He, N. Li, W. Li, X. Zhang, X. Zhang, Z. Liu and Q. Liu, *Sensors Actuators B Chem.*, 2021, **326**, 128850.

3 Q. Liu, Y. Ding, Y. Yang, L. Zhang, L. Sun, P. Chen and C. Gao, *Mater. Sci. Eng. C*, 2016, **59**, 445–453.

4 L. Zhu, F. Yang, C. Lou, X. Zhang and Y. Yang, *Microchim. Acta*, 2023, **190**, 339.

5 X. Zhao, S. Zhao, S. Li, X. Yao, X. Zhu, W. Chen, G. Fan, Z. Liu, Q. Liu and K. Yue, *ACS Appl. Nano Mater.*, 2021, **4**, 8706–8715.

6 Q. Liu, H. Li, Q. Zhao, R. Zhu, Y. Yang, Q. Jia, B. Bian and L. Zhuo, *Mater. Sci. Eng. C*, 2014, **41**, 142–151.

7 Q. Liu, P. Chen, Z. Xu, M. Chen, Y. Ding, K. Yue and J. Xu, *Sensors Actuators B Chem.*, 2017, **251**, 339–348.

8 Q. Liu, Y. Yang, X. Lv, Y. Ding, Y. Zhang, J. Jing and C. Xu, *Sensors Actuators B Chem.*, 2017, **240**, 726–734.

9 Q. Liu, Y. Yang, H. Li, R. Zhu, Q. Shao, S. Yang and J. Xu, *Biosens. Bioelectron.*, 2015, **64**, 147–153.

10 Y. Huang, M. Zhao, S. Han, Z. Lai, J. Yang, C. Tan, Q. Ma, Q. Lu, J. Chen, X. Zhang, Z. Zhang, B. Li, B. Chen, Y. Zong and H. Zhang, *Adv. Mater.*, 2017, **29**, 1700102.

11 C. Xu, Z. Yang, S. Zhang, X. Gao, L. Bao and Z. Meng, *Microchem. J.*, 2025, **210**, 112918.

12 S. N. Bhaduri, D. Ghosh, S. Chatterjee, R. Biswas, A. Bhaumik and P. Biswas, *J. Mater.*

Chem. B, 2023, **11**, 8956–8965.

13 D. Guo, C. Li, G. Liu, X. Luo and F. Wu, *ACS Sustain. Chem. Eng.*, 2021, **9**, 5412–5421.

14 C. Li, J. Zeng, D. Guo, L. Liu, L. Xiong, X. Luo, Z. Hu and F. Wu, *ACS Appl. Mater. Interfaces*, 2021, **13**, 49453–49461.

15 L. Liu, B. Zhao, X. Luo, L. Meng and F. Wu, *Food Anal. Methods*, 2023, **16**, 1477–1486.

16 L. Liao, S. Tong, X. Luo, G. Liu and F. Wu, *Microchim. Acta*, 2022, **189**, 384.